Hindawi
Advances in Materials Science and Engineering
Volume 2019, Article ID 5095120, 13 pages
https://doi.org/10.1155/2019/5095120

Research Article

Experimental Study on Seismic Strengthening of Confined Masonry Walls Using RPC

Xin Wang[1], **Shuming Li**[1], **Zhenli Wu**[2], **Fanyang Bu**[3], and **Fei Wang**[4]

[1]*School of Civil Engineering, Shandong Jianzhu University, Jinan 25000, China*
[2]*College of Civil Engineering, Tongji University, Shanghai 200092, China*
[3]*China Construction Science & Technology Co., Ltd., Beijing 10007, China*
[4]*Shandong Provincial Architectural Design & Research Institute Co., Ltd., Jinan 25000, China*

Correspondence should be addressed to Zhenli Wu; wzlsdd@tongji.edu.cn

Received 16 April 2019; Revised 22 July 2019; Accepted 16 August 2019; Published 23 September 2019

Academic Editor: Marián Palcut

Masonry structures without effective reinforcement are vulnerable to seismic excitation. An innovative strengthening technique was proposed for damaged and undamaged masonry walls. Six confined masonry units with two aspect ratios were tested under in-plane lateral cyclic loading, which consisted of two control walls, two original walls strengthened with reactive powder concrete (RPC-1), and two damaged walls repaired with RPC (RPC-2). The results of the specimens retrofitted with RPC demonstrated that the proposed technique significantly enhanced the seismic performance of masonry walls in terms of lateral strength, ductility, and energy dissipation. Furthermore, the two repaired specimens had a better distributed cracking pattern than the two strengthened specimens. The analysis of the results leads to a better understanding of the effect and mechanism of RPC seismic retrofitting for confined masonry walls.

1. Introduction

Recent earthquakes in mainland China, such as those happened in Wenchuan in 2008 and Yushu in 2010, have demonstrated the fragility of existing buildings under seismic excitation [1], particularly that of masonry buildings [2]. The risk presented by a large inventory of masonry structures in seismic zones had attracted many researchers in the development of retrofit methods that were appropriate for masonry structures. Over the past decades, a great variety of reinforcement methods have been proposed, studied, and implemented.

External steel jacket anchored by bolts [3–8] was proved to be an effective way to enhance flexural strength and ductility of concrete members. However, the bolted steel plates were prone to fail in local buckling and thus cannot be introduced to the strengthening of masonry walls [9]. Although additional transverse stiffeners were found to be able to restrain the local buckling phenomenon to some extent [10, 11], they exerted no significant influence on improving the overall strengthening performance.

The effectiveness of fiber-reinforced polymer technique for reinforced concrete members has been profoundly investigated [12–14]. This technique was also introduced to masonry members [15, 16] and overcomes some of the drawbacks of the aforementioned methods. It can be found that the in-plane lateral resistance and the displacement ductility were improved up to 135% and 374%, respectively, beneficial from fiber-reinforced polymer strengthening. However, organic epoxy resins, which were not friendly to environment and hazardous to human health, were always applied to bind fiber-reinforced polymers.

To address the issue, fiber-reinforced polymer strips and textile-reinforced concrete (TRC) [17] were respectively used on masonry walls, and both of them were able to improve the lateral bearing capacity and dissipation energy. Besides, the walls strengthened using TRC exhibited an increase of 185% in ductility but lower (175%) lateral strength when compared with the walls strengthened using FRP strips. Thus, further researches were required to provide new materials that can be compatible to masonry structures.

In recent years, the development of innovative materials [18–24] had validated the arising new strengthening techniques for masonry buildings. The in-plane compressive-shear tests and numerical analysis on adobe masonry walls retrofitted with polymeric grids inserted inside small thickness mortar jacketing were conducted by Garifano et al. [23], which demonstrated that the strengthening technique could improve both the ductility and lateral strength.

Reactive powder concrete (RPC) was an innovative concrete based on cementitious materials forming through microstructural enhancement [25]. RPC was readily applied in upgrading of reinforced concrete structures [26], and satisfactory results were obtained in the freeze-thaw cycle acceleration deterioration test due to its excellent mechanical properties. Moreover, a better adhesion was found between RPC and steel substrate when compared with other cementitious materials.

However, RPC has yet been applied to strengthen masonry structures, and most existing investigations were mainly focused on virgin masonry specimens strengthened with cement-based overlays. It was important to investigate the working mechanism and failure characteristics of damaged masonry walls retrofitted with the composite overlays.

Therefore, the present research will focus on the experimental investigation of the confined masonry walls strengthened or repaired using RPC coatings, subjected to a combination of constant vertical and cyclic horizontal loads, neglecting the inherent cyclical nature and the inertial effects of seismic actions. The RPC coatings for strengthening purposes was used as means of enhancing the weak bond between mortars and bricks, even improving the poor restraint of masonry panels. It mainly aims at studying the effectiveness of seismic retrofitting with RPC coatings for confined masonry walls, which can lead to a better understanding of the interaction of RPC coatings and masonry walls.

2. Materials and Methods

2.1. Description of Specimens. Four confined masonry walls were fabricated as shown in Figure 1. The aspect ratio of two walls was 1 : 1.5, and that of the other two was 1 : 2. The fired clay bricks with dimensions of 240 mm × 115 mm × 55 mm were used to build the walls. This type of masonry units was selected due to its wide application in the countryside of mainland China for constructing load-bearing masonry walls.

Previous researches [27–30] demonstrated that partial interaction was caused by the slippage between the steel jacket and substrate through the bolt connection, which led to a better strengthening effect. To achieve better collaboration between the masonry substrate and RPC coating, twenty-two 6 mm diameter U-shaped steel bars at a spacing of 250 mm were precast in the mortar joints as shown in Figure 1. The steel bars were characterized by average yield and ultimate strength values of 323 MPa and 435 MPa. Each wall was built in a reinforced concrete frame, which confined the masonry panel.

Four specimens, i.e., two control walls (CTRL-1.5 and CTRL-2) and two virgin specimens strengthened with RPC-1 coating in 20 mm thickness and named SW-1.5 and SW-2, were firstly tested to failure and analyzed. It was found that the strength and stiffness of RPC coating was excessively higher than that of masonry substrate, resulting in premature debonding of coatings. Therefore, the strength and thickness of the RPC coating was adjusted to RPC-2 in lower strength and 15 mm for a better compatibility with the masonry substrate in the repaired walls (RW-1.5 and RW-2).

In addition, the present research mainly focuses on the seismic behavior of confined wall before and after retrofitting with RPC coatings, rather than the comparison of the strengthening effectiveness of the proposed technique for the damaged and the original specimens.

Afterward, an inspection of damaged regions of the two control specimens, i.e. CTRL-1.5 and CTRL-2, was carried out. After the removal of the loose brick and mortars from the specimens, the masonry substrates were found to be not completely intact, and wide cracks existed. Before plastering the coating, the predamaged specimens were wetted. Then, the cracks and missing corners were filled with the RPC-2. The two control specimens were then rehabilitated using RPC-2 in 15 mm thickness and retested under the identical conditions. These two repaired specimens were named as RW-1.5 and RW-2. The reinforced parameters of all specimens are listed in Table 1.

2.2. Material Properties. According to Chinese codes, laboratory tests were conducted to assess the mechanical properties of fired clay bricks, mortar, concrete, and RPC matrix. The compressive tests of the fired clay bricks on $115 \times 55\,mm^2$ surface and on $240 \times 115\,mm^2$ surface were conducted. The mortar was characterized by conducting compressive tests on six 70.7 mm cubes at 28 days. Six 100 mm concrete cubes were tested after a 28-day curing period. The values of compressive strength of all materials used are presented in Table 2.

Normal tradition RPC matrix was characterized by dense microstructure, high strength (ranging from 200 MPa to 800 MPa), and prominent fluidity (slump was larger than 200 mm) [31, 32]. Thus, it was a difficult task to plaster the tradition matrix on the masonry substrate without mold. The masonry substrates were in a lower strength and stiffness when compared to the RPC matrix. The matrix as a coating must be compatible with the masonry substrate from physical, mechanical, and chemical standpoints.

In order to fit the features of masonry substrate, the RPC matrix should be adjusted to a lower strength and a lower fluidity and have good bond with the masonry substrate. For these reasons, two kinds of RPC were used in this research as shown in Table 3. RPC-1 was produced with Portland cement P.O. 52.5, while RPC-2 was obtained by reducing the strength grade of Portland cement to P.O. 42.5.

The sizes of sand used here was larger than that used in normal RPC mixture. Graded natural sand (the maximum size is 5 mm) was used to replace the whole volume of the fine sand as shown in Table 4. Silica fume, fly ash, and

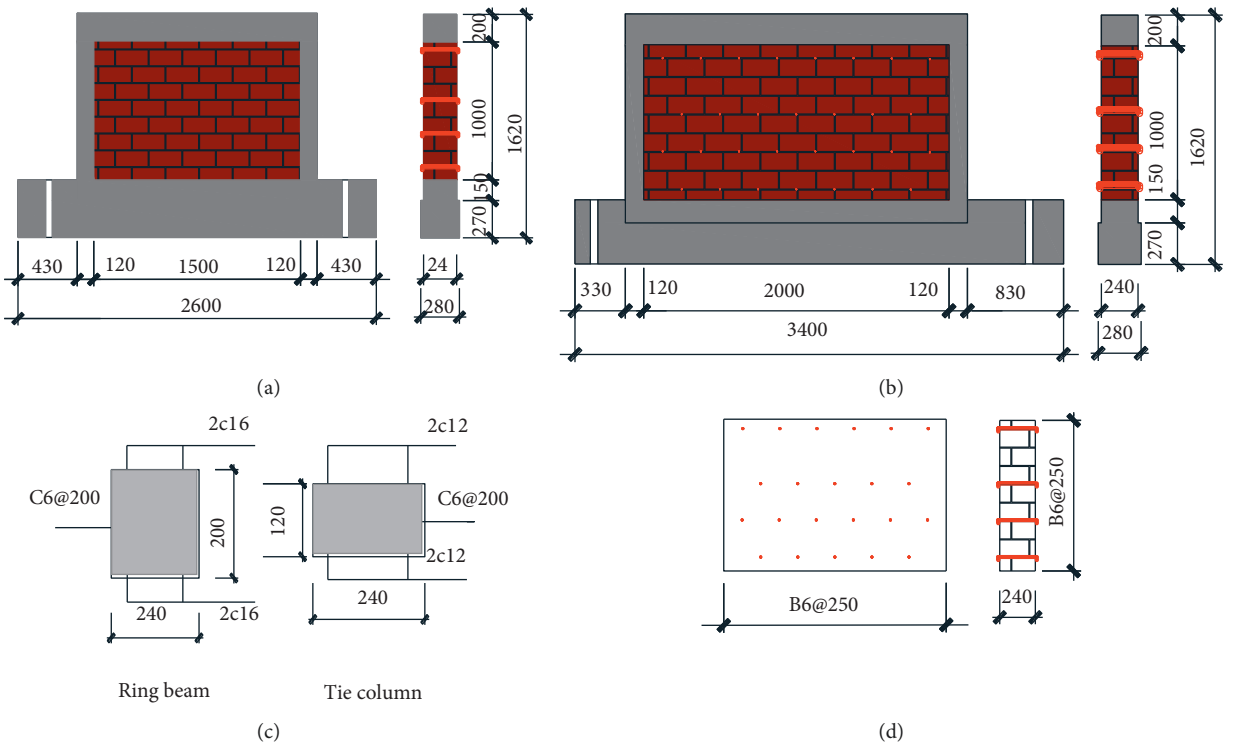

Figure 1: Description of the masonry units. (a) Aspect ratio of specimens in 1.5. (b) Aspect ratio of specimens in 2. (c) The description of the reinforced concrete members. (d) The position of U-shaped steel bars.

Table 1: The reinforced parameters of the specimens.

Specimen	Aspect ratio	Thickness	Material	Source of specimen
CTRL-1.5	1 : 1.5	—	—	Virgin
SW-1.5	1 : 1.5	20 mm	RPC-1	Virgin
RW-1.5	1 : 1.5	15 mm	RPC-2	Tested CTRL-1.5
CTRL-2	1 : 2	—	—	Virgin
SW-2	1 : 2	20 mm	RPC-1	Virgin
RW-2	1 : 2	15 mm	RPC-2	Tested CTRL-2

Table 2: Compressive strength of the materials.

Material	Fired clay brick		Mortar	Concrete	RPC-1 matrix	RPC-2 matrix
	Load on $115 \times 55\ mm^2$ surface	Load on $240 \times 115\ mm^2$ surface				
Compressive strength (MPa)	4.83	7.45	1.83	27.67	83.08	54.6

granulated blast furnace slag (GBFS) with particle size less than 45 μm, which was complied with Chinese standard, were used as fine aggregate. The chemical composition of silica fume, fly ash, and GBFS is presented in Table 5. The RPC matrix used in this research was manufactured using polypropylene fiber and steel fiber. The steel fiber in 13 mm length with the mean diameter of 0.2 mm was used to improve the tensile strength of RPC. The diameter of PP fibers was about 30 μm. The tensile strengths of steel fiber and PP fiber were 2850 MPa and 500 MPa, respectively.

The required RPC matrixes were mixed in two batches. The dry powder (fly ash, slag, and silica fume) and sand were initially blended. The water and water reducer were then added and followed by fibers. Six cubes in 70.7 mm were cured at the same ambience with the walls. The average 28-day compressive strength of RPC matrix gained from the tests on cubes is listed in Table 2.

The weight of water reducer was 0.34% of cement; weight method was used to design the mixtures, except for fiber, which was designed by volume.

Table 3: Mix proportions of RPC matrix (by weight ratio).

Material	Cement (grade)	Fly ash	Sand	Silica fume	Slag	Water reducer (%)	Water	Steel fiber (%)	Polypropylene fiber (%)
RPC-1	1 (P.O. 52.5)	0.3	2	0.4	0.3	0.34	0.5	1.5	0.5%
RPC-2	1 (P.O. 42.5)	0.3	2	0.4	0.3	0.34	0.5	1.5	0.5%

Table 4: River sand grading.

Sieve opening (mm)	<0.08	0.08	0.16	0.315	0.63	1.25	2.5	5
Cumulative % retained	2.88	5.39	9.42	23.7	52.31	80.39	98.35	100

Table 5: Chemical composition of FA, GGBS, and SF.

	Material	Cement (P.O. 42.5)	Cement (P.O. 52.5)	Fly ash	Silica fume	Slag
Chemical composition (%)	SiO_2	20.93	28.0	45	96.7	39.66
	Al_2O_3	5.12	7.62	34.8	—	12.94
	Fe_2O_3	2.8	4.84	8.8	—	—
	CaO	64.2	54.6	3.04	—	34.2
	MgO	3.4	1.4	0.61	—	6.94
	SO_3	2.0	1.7	—	—	0.72
	Na_2O	—	0.19			0.2
	K_2O	—	0.6			1.44
	Cl^-	0.04	0.03	—	0.01	—
	Loss in ignition	1.51	1.02	6.26	1.1	0.7

2.3. Test Setup. The low cyclic reversed loading test was a widely accepted method to assess the seismic performance of structural members, such as frames, shear walls, and masonry walls [16, 33, 34]. The specimens were tested in the Disaster Prevention and Mitigation Laboratory of Shandong Jianzhu University, China.

A steel frame with horizontal and vertical loading equipment was employed as shown in Figure 2. The boundary conditions of the specimens were similar to the cantilever wall with a fixed base and a top end free to in-plane movement. The footing beam was fastened to the strong floor using two steel rods with a diameter of 30 mm for preventing any possible slippage or lifting. In addition, both ends of the footing beam were blocked to avoid slippage.

The horizontal cycle load was imposed using a servo-hydraulic actuator following a displacement-control protocol. The allowable load capacity of the system is 1 MN both in tension and compression with a maximum displacement of 500 mm. The loads were measured by means of built-in force sensors of the actuator. To eliminate the influence of strain rate, the loading steps were conducted at a rate of 0.05 mm/s.

The loading history started with the lowest applied displacement and increment value of 0.4 mm until cracks appeared, which indicated the end of linear elastic stage of the specimen. The following displacement increment was set to be 2 times the previous values. Each increasing amplitude was exerted twice as shown in Figure 3. Lateral loading was continually imposed until the horizontal load falls by 15% accompanying with remark damages, such as penetrating cracks, crushing, and large-scale debonding.

In addition to the horizontal load, a vertical load equivalent to a uniform pressure of 0.5 MPa was exerted on a rigid beam using a hydraulic jack for simulating the gravity load of the upper stories of the building during the test. The rigid beam was mounted on the top of the specimens to transfer the vertical load. A load cell was connected to the hydraulic jack to monitor the change in the applied vertical load since the axial deformation of vertical members mainly depends on the axial compression ratio [35].

The horizontal displacements and deformations were measured with three linear variable differential transducers (LVDTs). LVDT 1 was set up to ensure that the specimen was fixed in the strong floor without slippage. LVDT 3 was assigned to measure the displacement at the top of the specimen, and LVDT 2 measured the displacement at the bottom of the specimen. The flexural and shear deformation contributions to the drift of the specimens were obtained by the difference of the two LVDTs.

Fifteen strain gauges of 120 mm length were mounted primarily for monitoring strains in vertical, horizontal, and diagonal direction at the characteristic sections of the specimens to measure shear and flexural deformations of RPC coating before cracking. Strains and displacements were all obtained with a data acquisition called DH-3816.

3. Experimental Observations

3.1. Failure Mode

3.1.1. Control Specimens. The damage patterns of the two control specimens are depicted in Figures 4(a) and 4(b), illustrating that the control specimens failed by shear with moderate ductile performance. The initial cracks of specimen CTRL-1.5 appeared at the bottom of the tie column while that of CTRL-2 appeared at the middle of the tie column. With increasing displacement, the cracks gradually

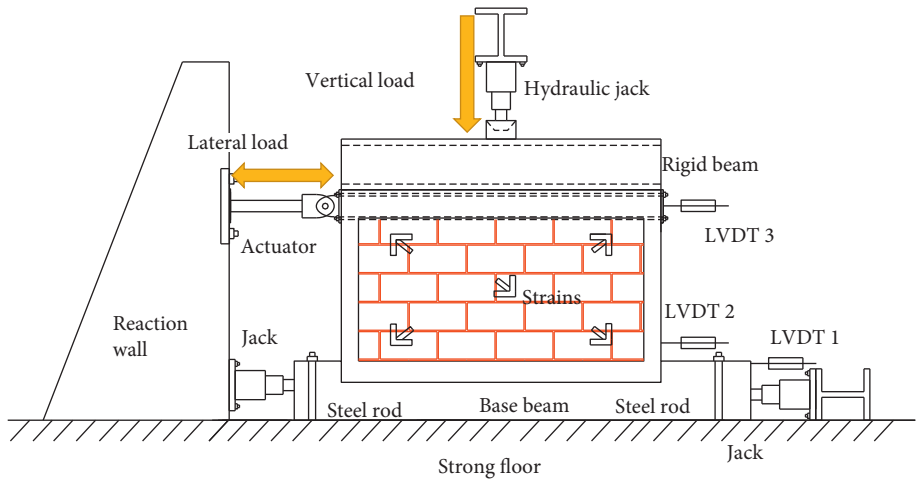

Figure 2: Test setup and instrumentation.

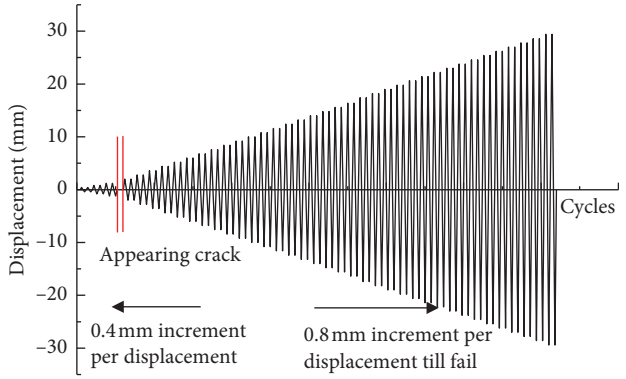

Figure 3: Horizontal displacement history of the actuator.

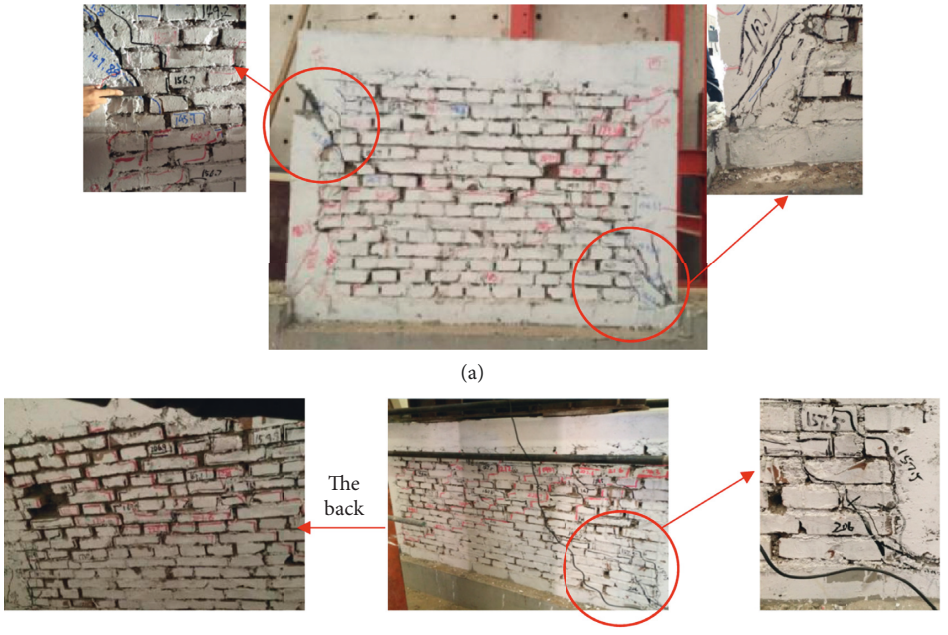

Figure 4: Crack pattern of the control specimens. (a) CTRL-1.5; (b) CTRL-2.

propagated to the masonry panel until formation of the wide stair-stepped cracking along their diagonal direction accompanied with toe crushing in the tie column. This occurred as a result of insufficient bond between mortars and bricks to bear the diagonal principal stress.

It is also shown that the main cracks in CTRL-1.5 initiated at the corner and propagated along the stair-stepped direction, while the spalling of bricks and mortars was mainly concentrated on the top of masonry panel in CTRL-2.

3.1.2. Strengthened Specimens. Both strengthened specimens exhibited a similar failure mode as shown in Figures 5(a) and 5(b). Analogous to that of the control specimens, fine cracks initiated at the lower corner of the tie columns in the strengthened specimens. When the crack widths became large enough to make the coating fail, the cracks propagated to the coatings with increasing displacement. This demonstrated that the coatings played an important role in enhancing the bond between bricks and mortars.

Afterward, the coating started to debond from the masonry substrate at the bottom corner of specimens. In addition, it can be significantly detected that the maximum loads at each displacement interval increased in a lower rate. This indicated that the interface action between the coating and masonry substrate played a critical role in the effectiveness promotion of this strengthening technique.

With increasing displacement, fine horizontal cracks appeared in the coating at the interface between the masonry wall and the concrete base beam. Besides, the coating substantially disconnected from the masonry substrate near the interface mainly due to the insufficient bond provided to anchor the coating. Herein, the peak load was reached.

Then, the debonding of coating was aggravated by the increasing displacement. Besides, a relative movement between the masonry substrate and RPC coatings can be observed during testing. This was because that the coatings could not deform compatibly with the masonry substrate due to its excessively higher stiffness. Besides, the bond was insufficient to deliver the interfacial shear stress between the coatings and the substrate. Thus, the RPC coating should be adjusted to fit the masonry substrate in the following tests.

Despite the fact that the postpeak decline of load reached 15% of the peak load, the tests were continued as the specimens did not endured severe damage. Finally, the specimens failed in a ductile manner. The coatings kept integrity with a small number of cracks during the entire test. This behavior was partly attributed to the U-shaped steel bars, which fixed the coating on the masonry substrate and transferred the shear force to a certain extent.

3.1.3. Repaired Specimens. Based on the results of the aforementioned specimens, RPC-2 was mixed and used in the repaired specimens. Both repaired specimens were characterized by a better distributed crack pattern on both sides along the diagonal direction, especially for the specimen RW-1.5, due to a better redistribution and development of tensile stress in the RPC coatings as shown in Figures 6(a) and 6(b). This means that the coating with thinner and lower strength was more compatible with masonry substrate.

From the perspective of cracks, the pulling out of PP fibers and steel fibers can be observed. Besides, a small number of U-shaped steel bars were protruding from the coating. Similar to the strengthened specimens, the repaired specimens started to disconnect from the substrate at the bottom of the tie column. As the debonding propagated to the masonry panel, the specimens reached the peak loads and hence fractured in a more ductile manner compared to the other specimens.

3.2. Load-Displacement Hysteresis Curves. The load-displacement hysteresis response was defined as a most important characteristic to evaluate the seismic behavior of a structural component. Because the energy dissipation efficiency and ductility capacity of the component can be evaluated from it during lateral cyclic loading. The load-displacement hysteresis curves for all specimens derived from the actuator are illustrated in Figure 7. Remarkable strength and stiffness degeneration were not observed in the second cycles for each displacement interval. The control specimens (CTRL-1.5 and CTRL-2) exhibited hysteresis loops with notable pinching, which was primarily attributed to the mortar joints cracking and toe crushing.

Compared to the control specimens, the loops of the strengthened specimens (SW-1.5 and SW-2) are obviously larger without notable pinching, while sharp strength deterioration and stiffness degradation exhibited. The specimens with different aspect ratios show the same trend of hysteresis behavior. The specimens with higher aspect ratio exhibited greater cracking load and peak load at the price of reducing ductility. It was worth noting that a sliding stage emerged in the strengthened specimens after the strength drop by the end of testing. It indicates that the integrity of the specimens was significantly enhanced by the RPC coating.

The hysteresis loops of the repaired specimens (RW-1.5 and RW-2) did not perform as well as the strengthened specimens mainly due to the existing damage in the bricks, mortar joints, and concrete. In terms of the hysteresis loops of the repaired and control specimens, it can be seen that the ultimate lateral load and deformation capacity of the repaired specimens were substantially improved with respect to their control counterparts, primarily resulting from the increased confinement between the tie column and the masonry panel. Besides, it was also because the shear force demand at the mortar joints was reduced as it was redistributed to the interface of masonry panel and RPC coating.

Finally, it could come to a conclusion that the proposed strengthening technique was effective in enhancing the hysteresis performance of the predamaged confined masonry wall.

4. Results and Discussion

In order to investigate the effectiveness of the proposed strengthening technique, the test results of the control,

Figure 5: Crack pattern of the strengthened specimens. (a) SW-1.5; (b) SW-2.

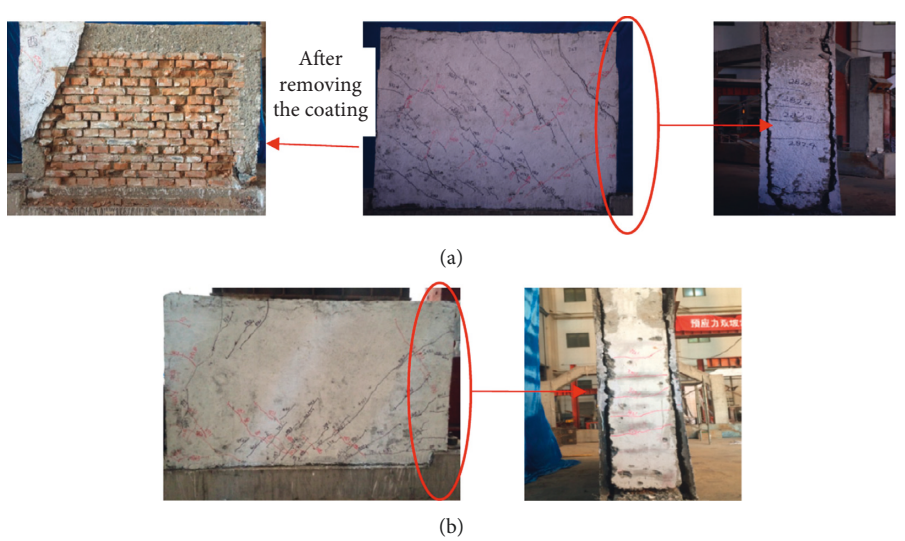

Figure 6: Crack pattern of the repaired specimens. (a) RW-1.5; (b) RW-2.

strengthened and repaired specimens will be compared in terms of seismic performance hereafter.

4.1. Load-Displacement Hysteresis Envelop Curves. The load-displacement envelop curves for the peak displacement point at each first reversal of cycles are depicted in Figure 8. The curves exhibited linear elastic responses in the first stage without visible cracks. Afterward, the slopes gradually degraded, and the behavior proceeded in-elastically until the peak load reached. Then, an abrupt drop (over 10%) of the strength occurred in the strengthened specimens mainly due to the extensive debonding of RPC coating, which might indicate a brittle failure in most cases.

However, it was interesting to find that the strengthened specimens exhibited a constant lateral load with increasing displacement to a higher stage, which indicated more ductile failure. Contrary to the strengthened specimens, a gradual descending was usually found in the envelop curves of the rest specimens.

By analyzing the experimental record and envelop curves, the cracking load (P_{cr}), cracking displacement (d_{cr}),

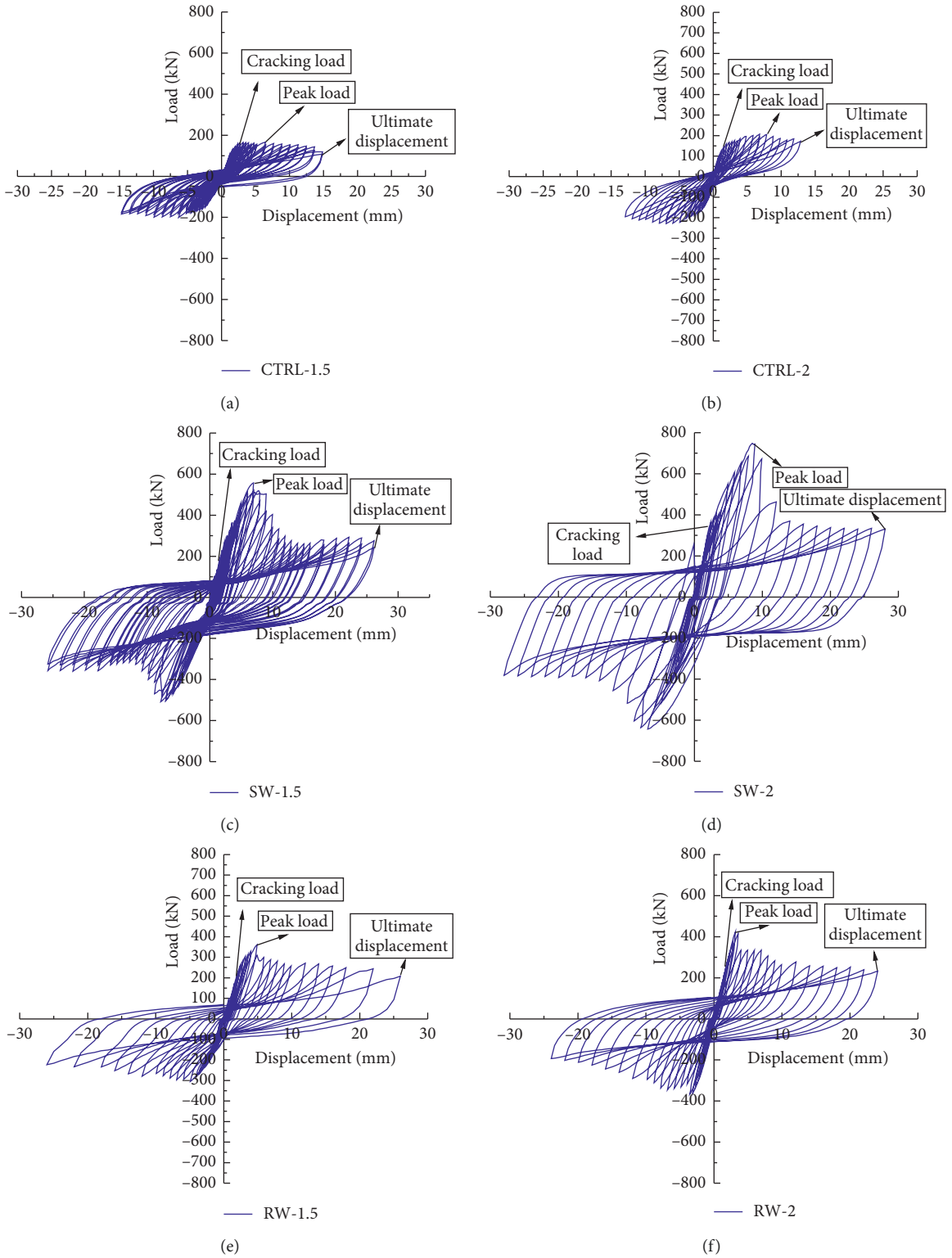

Figure 7: The load-displacement hysteresis curves derived from the actuator. (a) CTRL-1.5; (b) CTRL-2; (c) SW-1.5; (d) SW-2; (e) RW-1.5; (f) RW-2.

peak load (P_u), displacement at failure (d_u), expected ultimate load (P_{Eu}) [36], and ductility coefficient (μ) for all specimens on average value of pulling and pushing directions are listed in Table 6. Here, the ultimate displacement is the failure displacement, and the area is the gross section area of the specimens.

As seen from the table, the retrofitted (repaired and strengthened) specimens exhibited a substantial enhancement

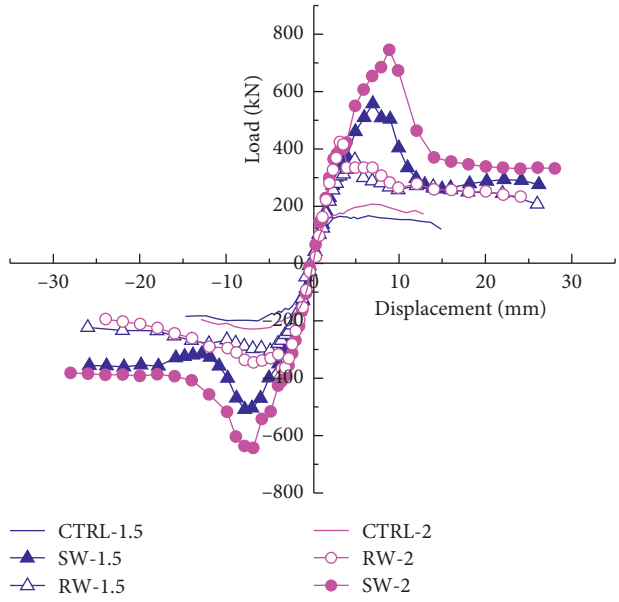

Figure 8: The load-displacement envelop curves of all specimens.

Table 6: Mechanical characteristics.

Specimen	Cracking load		Cracking displacement d_{cr} (mm)	Peak load				Displacement at failure d_u (mm)	$\mu = d_u/d_{cr}$	P_{Eu} (kN)
	P_{cr} (kN)	Increment (%)		P_u (kN)	Increment (%)	P_u area (%)	Increment (%)			
CTRL-1.5	162	—	2.8	184	—	442	—	15	5.4	172
SW-1.5	177	9.0	1.6	533	189.2	1094	147	26	16.3	—
RW-1.5	207	27.7	2	334	81.2	686	55	26	13.0	—
CTRL-2	152	—	1.6	218	—	406	—	13	8.1	197
SW-2	339	122.5	2.4	707	224.7	1170	188	28	11.7	—
RW-2	258	69.0	1.9	415	90.6	686	69	20	10.5	—

Note. The ultimate displacement is the failure displacement, the area is the gross section area of the specimens, and P_{Eu} is the expected ultimate load calculated according to the literature [36].

in ultimate load, ranging from 90% (RW-2) to 224% (SW-2) when compared to the control specimens. This indicates that the RPC coating can be regarded as an effective anchorage that can provide constraint for the original and damage masonry panel. Besides, the ultimate shear stress v_u (= P_u/Area) of the retrofitted specimens was enhanced for at least 55% due to the strengthening coating.

The strengthened specimens achieved significantly higher ultimate loads when compared to the repaired specimens. The ultimate shear stress of the strengthened specimens was at least 159% higher than that of the repaired specimens. This may be attributed to the fact that the masonry walls of repaired specimens were predamaged. Because the sum of ultimate shear stress in the control specimens and the repaired specimens was approximately identical to that of strengthened specimen. This may also be attributed to the fact that the masonry walls of the repaired specimens were strengthened with thinner and lower-strength RPC coating.

Needless to say, a more elaborate experimental investigation is still required to validate the above assumptions. However, the main purpose of the manuscript was to study the effectiveness of the proposed strengthening technique.

The ultimate shear stress increment of the retrofitted specimens with an aspect ratio of 1.5 was dropped by 11% to 41% relative to that of those with an aspect ratio of 2. Thus, it comes to the conclusion that reducing the aspect ratio can increase the ultimate load. However, the repaired specimen RW-1.5 exhibits the same ultimate displacement as the strengthened specimen SW-1.5.

4.2. Stiffness Ratio. Instantaneous stiffness of the wall was determined from the first cycle of each displacement interval as the slope of the peak-to-peak line using equation (1), as shown in Figure 9.

$$K_i = \frac{F_i^+ - F_i^-}{d_i^+ - d_i^-}, \tag{1}$$

When compared to the corresponding control specimens, increases between 8% and 33% were obtained for the initial stiffness of the repaired specimens and increases between 23% and 61% were achieved for that of the strengthened specimens. Thus, the strengthening technique can effectively enhance or recover the initial stiffness of

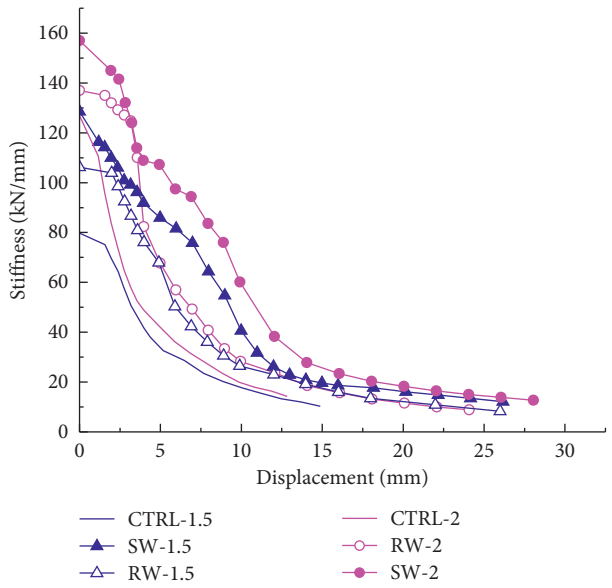

Figure 9: The stiffness degradation curves of all specimens.

confined masonry walls. This improvement in initial stiffness is mainly attributed to the collaborative work in RPC coating and masonry panel.

In addition, the retrofitted specimens shared the slower degradation in stiffness as compared to the control specimens. This can be attributed to the fibers have the ability to delay propagation of cracks and thus can maintain greater stiffness under loading.

The results indicate that the initial stiffness of the strengthened specimens was larger for about 15% (or 28%) than that of the corresponding repaired specimens, while the stiffness degradation rates were relatively lower. This can be explained by the fact that the masonry substrate of the repaired specimens was already damaged under lateral cyclic loading. It may also be attribute to higher strength and thicker coating of the strengthened specimens. Thus, it is difficult to assess the influence of the strengthening technique on the damaged and undamaged specimens by the stiffness.

The results also indicate that increasing the aspect ratio can significantly improve the stiffness of the specimens. The improvement in stiffness controls the lateral resistant capacity and decreases the damages exerted on the structures.

4.3. Ductility. The ductility was calculated using the ultimate displacement divided by the cracking displacement. As shown in Table 3, the ductility coefficient (μ) of the strengthened specimen (SW-1.5) reached a value of 16.3 due to a considerable debonding of RPC coating. The ductility coefficient of the damaged specimens repaired with RPC-2 was reduced by 10% and 20% when compared to that of the original strengthened specimens. The results also indicated that the control specimen with lower aspect ratio has a lower ductility factor, and the retrofitted specimens with lower aspect ratio have a higher ductility coefficient.

4.4. Energy Dissipation. The total energy dissipation of confined masonry walls consists of (1) energy dissipated by the interaction between the RPC coating and the masonry panel, (2) energy dissipated by friction along existing cracks in mortar joints, and (3) energy dissipated during the forming of new cracks and the crushing of the bricks and concrete.

The energy dissipation (E_p) was calculated by the area enclosed in an entire hysteresis loop at the first cycle of each displacement interval as shown in Figure 10. The energy dissipation curves were basically in a linear growth. The retrofitted specimens SW-1.5, SW-2, RW-1.5, and RW-2 dissipated more total energy than the corresponding control specimens up to 485%, 636%, 310% and 375%, respectively. It is evident that the control specimens performed a lower ductile behavior compared to the retrofitted specimens. More energy was dissipated by the strengthened specimens with respect to their repaired counterparts since the existing cracks in the repaired specimens had already dissipated some energies prior repairing.

4.5. Equivalent Viscous Damping Ratio. The equivalent viscous damping ratio (h_e) is commonly selected to quantify the energy dissipation by a structural component under seismic state by using

$$h_e = \frac{E_p}{2\pi E_e}, \tag{2}$$

where E_e is the potential elastic energy by an equivalent linear system when the maximum displacement is reached under static condition as shown in Figure 10.

The damping ratio versus displacement curves for all specimens is depicted in Figure 11. It can be found that the curves of the control specimens are basically in coincidence with a horizontal segment due to pinching effect and strength reduction, which was caused by shear failure of the

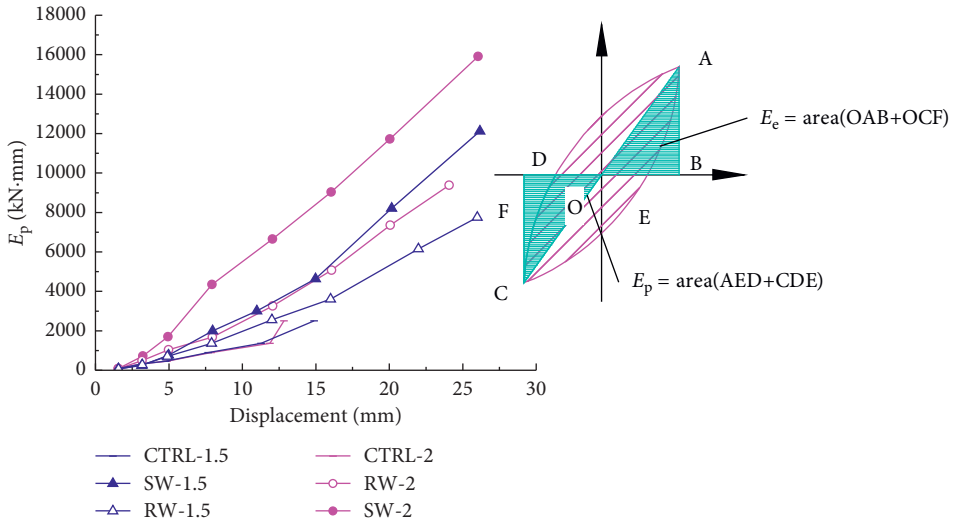

Figure 10: The energy dissipation curves of all specimens.

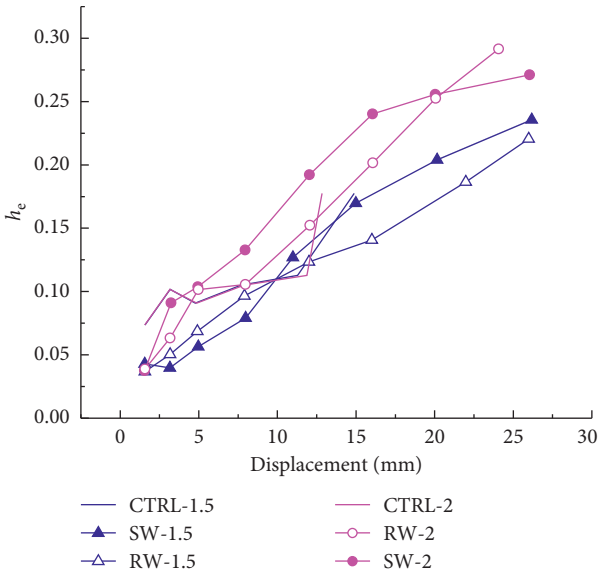

Figure 11: The equivalent viscous damping ratio of all specimens.

wall. The results show that the damping ratio of the retrofitted specimens increased at a near-linear trend. This may be attributed to the interaction between RPC coating and masonry panel, thus increasing the area of hysteresis loops without notably pinching effect. The damping ratios in the control specimens were limited to 17.5% and those values in retrofitted specimens were increased to 30%. The increase in damping ratio reflected the increasing displacement, development of cracks, crushing of bricks and mortar joints, and debonding of coating.

5. Conclusions

The behavior of confined masonry specimens upgraded using a modified "reactive powder concrete" was investigated. Six full-scale masonry specimens, including damaged and original specimens, were tested by applying a constant vertical load and a horizontal cyclic load of increasing amplitudes. Lateral bearing capacity, stiffness ratio, ductility, energy dissipation capacity, and equivalent viscous damping ratio were investigated. The main conclusions are as follows:

(1) The proposed strengthening technique did not change the failure mode, but significantly postponed the shear failure and enhanced the bond between mortars and bricks, and improved the constraint between concrete frame and masonry panel.

(2) The proposed strengthening technique was demonstrated to be able to significantly improve the seismic behavior of the undamaged and damaged masonry walls in terms of the parameters mentioned above.

(3) The pinching of the hysteretic curves was basically eliminated in the retrofitted specimens, and the total energy dissipations were increased 485%, 636%, 310%, and 375% for specimens SW-1.5, SW-2, RW-1.5, and RW-2, respectively, when compared to their corresponding control specimens.

(4) The ultimate loads for specimens SW-1.5, SW-2, RW-1.5, and RW-2 were increased by 189.2%, 224.7%, 81.2% and 90.6%, respectively, when compared to the corresponding control specimens.

(5) The magnitudes of average ductility were increased by 171% and 81% for the retrofitted specimens with the aspect ratio of 1 : 1.5 and 1 : 2, respectively, when compared to the corresponding control specimens.

(6) The initial stiffness of the repaired specimens was effectively recovered by the strengthening technique.

Finally, the comparisons of the effectiveness between the repaired specimens using damaged walls and the strengthened specimens using original walls were mainly speculated due to limited experimental conditions in this research. Further researches are required.

Data Availability

The data used to support the findings of this study are available from the corresponding author upon request.

Conflicts of Interest

The authors declare that there are no conflicts of interest regarding the publication of this paper.

References

[1] J. J. Tai, J. H. Deng, F. Chen, and J. B. Wei, "Characterization of surface rupture and structural damage in Hongkou town during Wenchuan earthquake," *Journal of Earthquake and Tsunami*, vol. 5, no. 4, pp. 363–387, 2011.

[2] M. Zhang and Y. Jin, "Building damage in Dujiangyan during Wenchuan earthquake," *Earthquake Engineering and Engineering Vibration*, vol. 7, no. 3, pp. 263–269, 2008.

[3] R. K. L. Su, L. Z. Li, and S. H. Lo, "Shear transfer in bolted side-plated reinforced concrete beams," *Engineering Structures*, vol. 56, no. 11, pp. 1372–1383, 2013.

[4] L. Z. Li, Z. W. Cai, Z. D. Lu, X. L. Zhang, and L. Wang, "Shear performance of bolted side-plated reinforced concrete beams," *Engineering Structures*, vol. 144, no. 8, pp. 73–87, 2017.

[5] J. Zhou and L. Wang, "Repair of fire-damaged reinforced concrete members with axial load: a review," *Sustainability*, vol. 11, no. 4, p. 963, 2019.

[6] L. Li, X. Liu, Y. Luo, M. Su, and J. Zhu, "Flexural performance of bolted-side-plated RC beams with buckling restraining," *ACI Structural Journal*, vol. 116, no. 2, pp. 77–87, 2019.

[7] C.-J. Jiang, Z.-D. Lu, and L.-Z. Li, "Shear performance of fire-damaged reinforced concrete beams repaired by a bolted side-plating technique," *Journal of Structural Engineering*, vol. 143, no. 5, article 04017007, 2017.

[8] L. Z. Li, Z. L. Wu, J. T. Yu, X. Wang, J. X. Zhang, and Z. D. Lu, "Numerical simulation of the shear capacity of bolted side-plated RC beams," *Engineering Structures*, vol. 171, no. 9, pp. 373–384, 2018.

[9] S. H. Farooq, M. Ilyas, and A. Ghaffar, "Technique for strengthening of masonry wall panels using steel strips," *Asian Journal of Civil Engineering (Building and Housing)*, vol. 6, no. 7, pp. 621–638, 2006.

[10] L. Z. Li, C. J. Jiang, L. J. Jia, and Z. D. Lu, "Local buckling of bolted steel plates with different stiffener configuration," *Engineering Structures*, vol. 119, no. 7, pp. 186–197, 2016.

[11] X. L. Xu, Z. D. Lu, L. Z. Li, and C. J. Jiang, "Numerical study on the local buckling behaviour of bolted steel plates in steel jacketing," *Advances in Materials Science and Engineering*, vol. 2017, Article ID 1352084, 15 pages, 2017.

[12] J. Yu, K. Liu, L.-z. Li, Y. Wang, K. Yu, and Q. Xu, "A simplified method to predict the fire resistance of RC Beams strengthened with near-surface mounted CFRP," *Composite Structures*, vol. 193, no. 6, pp. 1–7, 2018.

[13] L.-J. Ouyang, W.-Y. Gao, B. Zhen, and Z.-D. Lu, "Seismic retrofit of square reinforced concrete columns using basalt and carbon fiber-reinforced polymer sheets: a comparative study," *Composite Structures*, vol. 162, pp. 294–307, 2017.

[14] L. F. Zhang, W. Q. Liu, G. Q. Sun, L. Wang, and L. Z. Li, "Two-dimensional modeling of thermomechanical responses of rectangular GFRP profiles exposed to fire," *Advances in Materials Science and Engineering*, vol. 2017, Article ID 1705915, 17 pages, 2017.

[15] A. Mosallam and S. Banerjee, "Enhancement in in-plane shear capacity of unreinforced masonry (URM) walls strengthened with fiber reinforced polymer composites," *Composites Part B: Engineering*, vol. 42, no. 6, pp. 1657–1670, 2011.

[16] M. A. Elgawady, P. Lestuzzi, and M. Badoux, "Aseismic retrofitting of unreinforced masonry walls using FRP," *Composites Part B: Engineering*, vol. 37, no. 2-3, pp. 148–162, 2006.

[17] T.-L. Bui, A. Si Larbi, N. Reboul, and E. Ferrier, "Shear behaviour of masonry walls strengthened by external bonded FRP and TRC," *Composite Structures*, vol. 132, no. 11, pp. 923–932, 2015.

[18] K. Yu, L. Li, J. Yu, J. Xiao, J. Ye, and Y. Wang, "Feasibility of using ultra-high ductility cementitious composites for concrete structures without steel rebar," *Engineering Structures*, vol. 170, no. 9, pp. 11–20, 2018.

[19] K. Yu, L. Li, J. Yu, Y. Wang, J. Ye, and Q. Xu, "Direct tensile properties of engineered cementitious composites: a review," *Construction and Building Materials*, vol. 165, no. 3, pp. 346–362, 2018.

[20] M.-T. Chen and B. Young, "Material properties and structural behavior of cold-formed steel elliptical hollow section stub columns," *Thin-Walled Structures*, vol. 134, no. 1, pp. 111–126, 2019.

[21] F. Parisi, I. Iovinella, A. Balsamo, N. Augenti, and A. Prota, "In-plane behaviour of tuff masonry strengthened with inorganic matrix-grid composites," *Composites Part B: Engineering*, vol. 45, no. 1, pp. 1657–1666, 2013.

[22] L. Li, Z. Cai, K. Yu, Y. X. Zhang, and Y. Ding, "Performance-based design of all-grade strain hardening cementitious composites with compressive strengths from 40 MPa to 120 MPa," *Cement and Concrete Composites*, vol. 97, no. 4, pp. 202–217, 2019.

[23] A. Garofano, F. Ceroni, and M. Pecce, "Modelling of the in-plane behaviour of masonry walls strengthened with polymeric grids embedded in cementitious mortar layers," *Composites Part B: Engineering*, vol. 85, no. 2, pp. 243–258, 2016.

[24] M. Lai, L. Hanzic, and J. C. M. Ho, "Fillers to improve passing ability of concrete," *Structural Concrete*, vol. 20, no. 1, pp. 185–197, 2019.

[25] H. Yazıcı, M. Y. Yardımcı, S. Aydın, and A. Ş. Karabulut, "Mechanical properties of reactive powder concrete containing mineral admixtures under different curing regimes," *Construction and Building Materials*, vol. 23, no. 3, pp. 1223–1231, 2009.

[26] M.-G. Lee, Y.-C. Wang, and C.-T. Chiu, "A preliminary study of reactive powder concrete as a new repair material," *Construction and Building Materials*, vol. 21, no. 1, pp. 182–189, 2007.

[27] R. K. L. Su, L. Z. Li, and S. H. Lo, "Longitudinal partial interaction in bolted side-plated reinforced concrete beams," *Advances in Structural Engineering*, vol. 17, no. 7, pp. 921–936, 2014.

[28] S. H. Lo, L. Li, and R. K. L. Su, "Optimization of partial interaction in bolted side-plated reinforced concrete beams," *Computers and Structures*, vol. 131, no. 7, pp. 70–80, 2014.

[29] L.-Z. Li, C.-J. Jiang, R. K.-L. Su, and S.-H. Lo, "A piecewise linear transverse shear transfer model for bolted side-plated beams," *Structural Engineering and Mechanics*, vol. 62, no. 4, pp. 443–453, 2017.

[30] L.-Z. Li, C.-J. Jiang, R. K.-L. Su, and S.-H. Lo, "Design of bolted side-plated reinforced-concrete beams with partial interaction," *Proceedings of the Institution of Civil Engineers-Structures and Buildings*, vol. 169, no. 2, pp. 81–95, 2016.

[31] N.-H. Yi, J.-H. J. Kim, T.-S. Han, Y.-G. Cho, and J. H. Lee, "Blast-resistant characteristics of ultra-high strength concrete and reactive powder concrete," *Construction and Building Materials*, vol. 28, no. 1, pp. 694–707, 2012.

[32] C.-T. Liu and J.-S. Huang, "Fire performance of highly flowable reactive powder concrete," *Construction and Building Materials*, vol. 23, no. 5, pp. 2072–2079, 2009.

[33] L.-Z. Li, X. Liu, J.-T. Yu et al., "Experimental study on seismic performance of post-fire reinforced concrete frames," *Engineering Structures*, vol. 179, no. 1, pp. 161–173, 2019.

[34] J. Paterson and D. Mitchell, "Seismic retrofit of shear walls with headed bars and carbon fiber wrap," *Journal of Structural Engineering*, vol. 129, no. 5, pp. 606–614, 2003.

[35] J. Yu, K. Zhan, L. Li, K. Yu, and K. Q. Yu, "Using XFEM to model the effect of different axial compression on the hysteretic behaviour of the flexure-dominant RC columns," *The Structural Design of Tall and Special Buildings*, vol. 27, no. 8, p. e1465, 2018.

[36] M. Tomaževič and I. Klemenc, "Seismic behaviour of confined masonry walls," *Earthquake Engineering & Structural Dynamics*, vol. 26, no. 10, pp. 1059–1071, 2015.